IX CONGRESSO BRASILEIRO DE
ENGENHARIA E CIÊNCIAS TÉRMICAS

9th BRAZILIAN CONGRESS OF THERMAL
ENGINEERING AND SCIENCES

Paper CIT02-0587

NUMERICAL PREDICTION OF TURBULENT FLOWS AROUND A SQUARE CYLINDER WITH DIFFERENT TURBULENCE MODELS

Odenir de Almeida
odenir.almeida@embraer.com.br
Embraer – Empresa Brasileira de Aeronáutica S.A.
Av. Brigadeiro Faria Lima, 2170 – São José dos Campos S.P – Brazil, 12227-901

Sérgio Said Mansur
UNESP Ilha Solteira - Departamento de Engenharia Mecânica
15385-000 – Ilha Solteira, SP – Brazil

Aristeu da Silveira Neto
UFU – Faculdade de Engenharia Mecânica
38400-092 – Uberlândia, MG – Brazil

Abstract. *The two-dimensional vortex shedding behind a square cylinder at high Reynolds numbers has been simulated in this work. Three different turbulence models – Smagorinsky (LES), k-ε standard and k-ε realizable – have been employed, and their respective performance was evaluated by a comparative way. Numerical calculations have been carried out by means of a finite-volume method employing a structured grid. An incompressible SIMPLEC algorithm has been employed for the velocity-pressure coupling, and a third-order QUICK scheme has been used for the treatment of convective terms. Particularly in the LES case, the influence of Smagorinsky constant on the flow field has been investigated. The numerical results, expressed in terms of quantitative parameters as Strouhal number and time-averaged velocity, are compared with experimental and numerical data from other authors. A qualitative study of the flow patterns is also evaluated by means of streamlines and vorticity contours analysis.*

Keywords. *square cylinder, vortex shedding, numerical simulation, large eddy simulation, k-ε model*

1. Introduction

In principle, it is possible to simulate any turbulent flow by solving directly the Navier-Stokes equations with appropriate boundary conditions and using a suitable numerical procedure. In this case the calculation is called *Direct Numerical Simulation* (DNS), but it is rarely done because in the most times the computational effort is prohibitive, especially for high Reynolds numbers. In front of this difficulty, two alternative ways have been developed for predicting turbulent flows encountered in practical engineering applications: *Classical Turbulence Modeling* and *Large Eddy Simulation* (LES). The first approach implies in mathematical manipulation of the governing equations by means of average – or filtering – process, and employs a set of relations and equations to determine the unknown turbulent correlations, which have arisen from this treatment. On the other hand, the LES method involves direct simulation of large turbulent structures, and the use of sub-grid models to represent the effects of the smallest scales presents in the flow field.

In the last decades due to intensive research activity on turbulence in fluids, various types of models have been created or improved. For testing the new developments in this area some canonical flows are frequently used. In this context, the turbulent flow past around cylinders is a particularly adequate problem to validation of numerical models. In fact, the nature highly complex of the interaction among shears layers and large-scale periodicity of the vortex shedding becomes this kind of flow a challenge for the numerical prediction of the fluid motion.

In the literature, some authors present studies about the performance of different turbulence models employed in the numerical solution of the flow past around square cylinders, as the notable works of Franke & Rodi (1991), Murakami (1993) and Rodi (1993).

Lee (1997) presents a numerical prediction of unsteady aerodynamic force on a square cylinder using k-ε turbulence models. In this study, the classical and improved k-ε models have been used and different numerical effects have been investigated as temporal and spatial resolutions, convection scheme choice and employ of distinct turbulence models. In summary, the author concluded that not only the turbulence model determines the quality of unsteady turbulence simulation, but also equally the numerical parameters associated.

Murakami & Iizuka (1999) presents an analysis of turbulent flow past square cylinder using dynamic LES three-dimensional. A comparison between the Smagorinsky (S) and Dynamic models (DS) is accounting in order to identify advantages and disadvantages of DS model. The results obtained for lift and drag force and velocity distributions from the various sub-grid-scale models (SGS) were compared with experimental data showing some discrepancies among the methodologies employed.

Recently, special attention has been given to application of Large Eddy Simulation and k-ε turbulence models in structural and wind engineering, considering the turbulent flows past bluff bodies. Yu & Kareem (1997) investigated numerically, using LES, both two-dimensional and three-dimensional flow surrounding a rigid rectangular prism for high Reynolds numbers. Their results are based in the velocity distribution and pressure fields, showing a very good agreement with available experimental data. In this work, the authors concluded that the refinement of mesh in 3D LES simulation is a very important factor to obtain physically consistent results. The use of a coarse mesh, in this case, gives inferior results to the 2D LES simulation with refined meshes.

The purpose of the present work is to compare and to test the three more utilized models in numerical simulations of turbulent motion – sub-grid-scale Smagorinsky model, *k*-ε standard and *k*-ε realizable – to predict the 2D flow past around a square cylinder at high Reynolds numbers (1.4×10^4 and 2.2×10^4). The numerical results are compared with experimental ones from Durão *et al.* (1988) and Lyn *et al.* (1995) showing some relevant discrepancies among the models investigated.

2. Numerical Methodology

2.1 Problem Formulation

In this work, the flow was assumed to be turbulent, unsteady and two-dimensional, with constant fluid properties. A rectangular domain structured on the Cartesian coordinate system with meshes non-uniformly distributed forms the computational grid. The numerical simulations have been accomplished by the numerical code FLUENT®5.3 employing the *Smagorinsky* LES, *k*-ε standard and *k*-ε realizable turbulence model. In all simulations, it have been utilized an incompressible SIMPLEC finite-volume algorithm (Patankar & Spalding, 1972) associated to QUICK scheme (Leonard, 1979) for discretization of the convective terms in the Navier-Stokes equations. A second-order central differences scheme has been used for the diffusive terms.

Figure 1 shows the computational domain and mesh resolution. The domain dimensions were accomplished taking into account the characteristic length of the cylinder (*B*). The boundary conditions have been set as follows: At the upstream boundary, the inlet flow has been assumed to be uniform for all cases. At the outlet, a zero gradient boundary condition for *U* and the prescribed velocity zero for *V* has been used. At the upper and lower boundaries the symmetry conditions have been used, simulating a frictionless wall ($V = \partial U/\partial y = 0$).

A marching time step of $\Delta t = 10^{-4}$ s was used employing a second-order fully implicit scheme for the unsteady terms. A non-dimensional time was defined by $t^* = t \cdot U_\infty / B$, where t is the computational time. The solution has advanced until the fully developed vortex street has been obtained characterized for a periodic variation in the average variables of the flow field. The simulations were conducted in a PC 700 MHz (0.88 Gflops peak performance) taking about 90 CPU hours for each case.

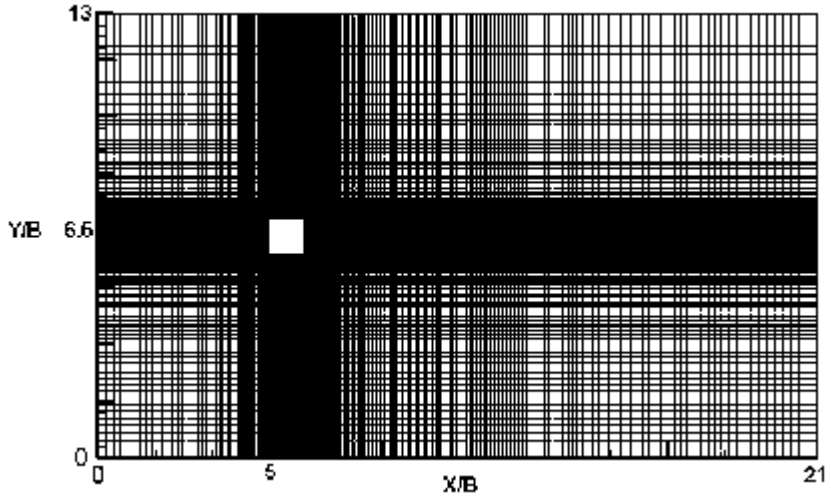

Figure 1. Computational grid (240×160) mesh resolution – ($21B \times 13B$) domain dimension.

For the calculation of Strouhal number, it was placed a numerical probe in the wake of the cylinder on the centerline at position-distanced 4*B* behind the obstacle. The temporal evolution of the *y*-component velocity was registered in the fully periodic regime of vortex formation and the numerical signal was processed by means of the Fast Fourier Transform (FFT), resulting in the fundamental frequency of vortex shedding.

2.2 Near-Wall Treatment

In the bluff bodies simulations at high Reynolds numbers the use of different approaches have been tested for handling the near-wall region, where there is large velocity gradients. In fact, very close to the wall, viscous damping reduces the tangential velocity fluctuations, while kinematics blocking reduces the normal fluctuations. In order to represents a correct velocity distribution near-wall the well known near-wall treatment has been frequently used for turbulent flows.

In this study, the all simulations were accomplished with the standard wall functions in FLUENT, proposed by Launder & Spalding (1974). The law-of-the-wall for mean velocity yields:

$$\frac{U_P C_\mu^{1/4} k_P^{1/2}}{\tau_w / \rho} = \frac{1}{k} \ln(E y^*) \tag{1}$$

where,

$$y^* = \frac{\rho\, C_\mu^{1/4} k_P^{1/2} y_P}{\mu} \tag{2}$$

with the von Kármán constant (k) equal to 0.42 and the constant empirical (E) equal to 9.81. The variables U_P, k_P and y_P are respectively the mean velocity of the fluid at point P, turbulent kinetic energy at point P and distance from point P to the wall. The logarithmic law for mean velocity is known to be valid for $y^* > 30 \sim 60$. In FLUENT numerical code, the log-law is employed when $y^* > 11.225$. It is important to emphasize that the logarithmic law is not well adequate to predict recirculating flows with shear layer interactions and that it was used in this work as a baseline approach. Further analysis of this problem needs to be made with improved wall functions.

3. Turbulence Models

3.1 Smagorinsky sub-grid-scale model (LES)

The incompressible governing equations employed for LES are obtained by filtering the time-dependent Navier-Stokes equations. As showed by Silveira Neto (1991), this approach leads to follows equations:

$$\frac{\partial}{\partial x_i}(\bar{u}_i) = 0 \tag{3}$$

$$\frac{\partial}{\partial t}(\bar{u}_i) + \frac{\partial}{\partial x_j}(\bar{u}_i \bar{u}_j) = -\frac{1}{\rho}\frac{\partial \bar{p}}{\partial x_i} + \frac{\partial}{\partial x_j}\left\{\nu\left(\frac{\partial \bar{u}_i}{\partial x_j} + \frac{\partial \bar{u}_j}{\partial x_i}\right) + \tau_{ij}\right\} \tag{4}$$

where τ_{ij} is the sub-grid-scale stress, defined by:

$$\tau_{ij} \equiv \overline{u_i u_j} - \bar{u}_i \bar{u}_j \tag{5}$$

The sub-grid-scale stresses resulting from the filtering operation are unknown, and require modeling. In this work, the Smagorinsky model is used to evaluate the sub-grid-scale viscosity through the Boussinesq hypothesis:

$$\tau_{ij} - \frac{1}{3}\tau_{kk}\delta_{ij} = -2\mu_t \bar{S}_{ij} \tag{6}$$

where μ_t is the sub-grid-scale turbulent viscosity, and $\bar{S}_{ij}$ is the rate-of-strain tensor for the resolved scale defined by:

$$\bar{S}_{ij} = \frac{1}{2}\left(\frac{\partial \bar{u}_i}{\partial x_j} + \frac{\partial \bar{u}_j}{\partial x_i} \right) \tag{7}$$

$$\mu_t = \rho L^2_S \left| \bar{S} \right| \tag{8}$$

where L_S is the mixing length for sub-grid scales and $\left|\bar{S}\right| \equiv \sqrt{2\bar{S}_{ij}\bar{S}_{ij}}$. The value L_S is computed using:

$$L_S = \min\left(kd, C_S V^{1/3}\right) \tag{9}$$

where k = 0.42, d is the distance to the closest wall, and V is the volume of the computational cell. The parameter $C_S \cong 0.2$ is the Smagorinsky constant determined analytically by Lilly in 1966.

3.2 k-ε standard

The standard k-ε model is a semi-empirical turbulence model based on model transport equations for the turbulent kinetic energy (k) and its dissipation rate (ε) obtained from the following equations:

$$\rho \frac{Dk}{Dt} = \frac{\partial}{\partial x_i}\left[\left(\mu + \frac{\mu_t}{\sigma_k} \right) \frac{\partial k}{\partial x_i} \right] + G_k - \rho\varepsilon \tag{10}$$

$$\rho \frac{D\varepsilon}{Dt} = \frac{\partial}{\partial x_i}\left[\left(\mu + \frac{\mu_t}{\sigma_\varepsilon} \right) \frac{\partial \varepsilon}{\partial x_i} \right] + C_{1\varepsilon} \frac{\varepsilon}{k}\left(G_k\right) - C_{2\,\varepsilon} \rho \frac{\varepsilon^2}{k} \tag{11}$$

In these equations, G_k represents the generation of turbulent kinetic energy due to the mean velocity gradients:

$$G_k = \mu_t S^2 \tag{12}$$

where μ_t is the turbulent viscosity and S is the modulus of the mean rate-of-strain tensor.

In this model $C_{1\varepsilon}$, $C_{2\varepsilon}$, are empirical constants having the following default values:

$$C_{1\varepsilon} = 1.44 \quad C_{2\varepsilon} = 1.92 \tag{13}$$

The terms σ_k and σ_ε are the turbulent Prandtl numbers for k and ε, respectively with the following default values:

$$\sigma_k = 1.0 \qquad \sigma_\varepsilon = 1.3 \tag{14}$$

In the k-ε standard model the turbulent viscosity, μ_t is calculated combining k and ε:

$$\mu_t = \rho\, C_\mu \frac{k^2}{\varepsilon} \tag{15}$$

with $C_\mu = 0.09$.

3.3 k-ε realizable

The k-ε realizable model, proposed by Shih *et al.* (1995), was intended to improve some deficiencies in the k-ε standard model, as a fundamental defect to neglect rotation, anisotropy and non-equilibrium effects. Basically, in this model, two important characteristics were incorporated. A new eddy-viscosity formula involving a variable C_μ originally proposed by Reynolds (1987) and a new model equation for dissipation (ε) based on the dynamic equation of the mean-square vorticity fluctuation.

The transport equations for k and ε in the k-ε realizable are, respectively:

$$\rho \frac{Dk}{Dt} = \frac{\partial}{\partial x_i}\left[\left(\mu + \frac{\mu_t}{\sigma_k}\right)\frac{\partial k}{\partial x_i}\right] + G_k \tag{16}$$

$$\rho \frac{D\varepsilon}{Dt} = \frac{\partial}{\partial x_i}\left[\left(\mu + \frac{\mu_t}{\sigma_\varepsilon}\right)\frac{\partial \varepsilon}{\partial x_i}\right] + \rho C_1 S\varepsilon - \rho C_2 \frac{\varepsilon^2}{k + \sqrt{\nu\varepsilon}} \tag{17}$$

where:

$$C_1 = \max\left[0.43\ ,\ \frac{\eta}{\eta + 5}\right] \tag{18}$$

with $\eta = Sk/\varepsilon$.

The values C_1 e C_2 are constants and σ_k e σ_ε are the turbulent Prandtl number for *k* and ε respectively. Note that the k equation (Equation 17) is the same as that in the standard *k*-ε model, except for the models constants. However, the form of the ε equation is quite different from those in the standard k-ε models. One of the noteworthy features is that the production term in the ε equation does not involve the production of *k*; i.e., it does not contain the same G_k term as the other *k*-ε models. It is believed that the present form is a better way to represent the spectral energy transfer.

As in other *k*-ε models, the eddy viscosity is computed from Equation 16. The difference between the realizable *k*-ε model and the standard *k*-ε models is that C_m is no longer constant. It is computed from:

$$C_\mu = \frac{1}{A_0 + A_s \dfrac{U^* k}{\varepsilon}} \tag{19}$$

where:

$$U^* = \sqrt{S_{ij}S_{ij} + \tilde{\Omega}_{ij}\tilde{\Omega}_{ij}} \tag{20}$$

and

$$\tilde{\Omega}_{ij} = \Omega_{ij} - 2\varepsilon_{ijk} w_k\ ,\ \text{and} \quad \Omega_{ij} = \overline{\Omega}_{ij} - \varepsilon_{ijk} w_k \tag{21}$$

where $\overline{\Omega}_{ij}$ is the mean rate-of-rotation tensor viewed in a rotating reference frame with the angular velocity w_k. The model constants A_0 and A_s are given by:

$$A_0 = 4.04 \qquad A_s = \sqrt{6}\cos\phi \tag{22}$$

where:

$$\phi = \frac{1}{3}\arccos\left(\sqrt{6}W\right), \qquad W = \frac{S_{ij}S_{jk}S_{ki}}{\tilde{S}}\ , \qquad \tilde{S} = \sqrt{S_{ij}S_{ij}} \tag{23}$$

The model constants C_2, σ_k and σ_ε, have been established to ensure that the model performs well for certain canonical flows. The model constants are:

$$C_{1\varepsilon} = 1.44\ ,\quad C_2 = 1{,}9\ ,\qquad \sigma_k = 1.0\ ,\qquad \sigma_\varepsilon = 1.2 \tag{24}$$

4. Numerical Results

The numerical results are presented in terms of dimensionless parameters, such as the Reynolds number:

$$Re = U_\infty B/\nu \tag{25}$$

where U_∞ is the free stream velocity, *B* is the characteristic length of the cylinder and ν is the kinematics viscosity of fluid; and the Strouhal number, defined by the relationship:

$$St = fB / U_\infty \tag{26}$$

where f is the fundamental frequency of vortex shedding.

4.1 Flow Regime at Re = 1.4×10^4

Two simulations were conducted for this Reynolds number employing the Smagorinsky constant equal to 0.1 and 0.15. The results indicates a better performance with Cs = 0,1, however both simulations provided satisfactory data when compared with the experimental and numerical results in the literature. Table 1 presents the numerical calculus for the Strouhal number obtained with the different turbulence models. It worth noting that the values obtained with LES methodology were about 20% more than the data of Durão *et al.* (1988). In the same table, is evident that the results provided by the simulation without turbulence model is longer to predict correctly the value of the Strouhal number. Although the *k*-ε simulations have provided a closest value to experimental data for the parameter investigated, the further calculus not reveals the same trend.

Table 1. Strouhal number of a square cylinder at $Re = 1.4 \times 10^4$.

Configuration		Strouhal
Present work	Without turbulence model	0.2015
	k - ε standard	0.1359
	k - ε realizable	0.1425
	LES – Cs = 0.1	0.1668
	LES – Cs = 0.15	0.1834
Durão *et al.* (1988) – Experimental		0.1390

Figure 2 shows the longitudinal velocity distribution on the centerline at upstream and downstream of the cylinder. At the upstream, the velocity distribution is practically the same for all simulations under predicting the experimental values in the entry region. In this case, this discrepancy can be associated to turbulent decay (dissipation) before the cylinder. However, the major discrepancies are verified in the recirculation region behind the cylinder. The k - ε results were incapable to predict the length of recirculation bubble and the recovering of velocity at downstream. On the other hand, it is observed a much better prediction of this flow dynamics with the Smagorinsky model with Cs = 0.1.

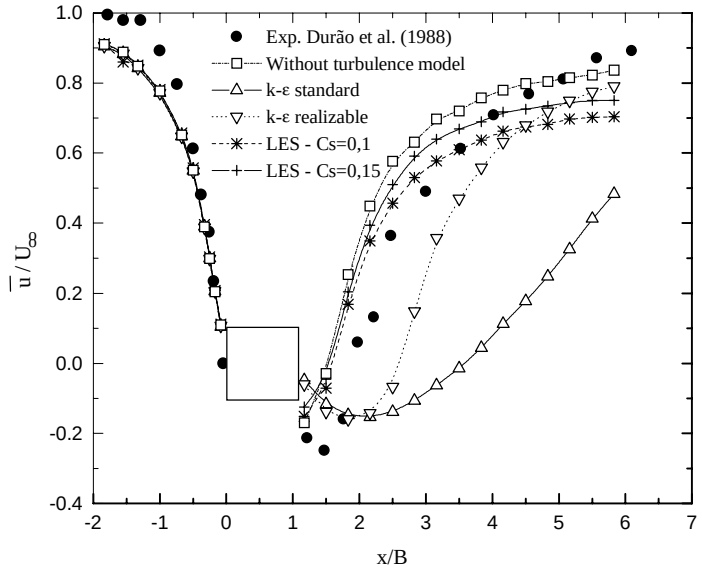

Figure 2. Longitudinal velocity distribution on the centerline at $Re = 1.4 \times 10^4$.

Figure 3 displays the longitudinal ($\overline{u'^2}$) and normal ($\overline{v'^2}$) velocity fluctuations also on the centerline. Here, it is most evident the better results provided by LES methodology, as compared with both standard and realizable *k*-ε simulations. Again, the numerical results are closest to experimental data for the Smagorinsky constant equal to 0.1.

Figure 4 shows the energy spectrum obtained from the transversal velocity fluctuation v' signal captured in the wake for the simulations with and without the Smagorinsky model. This plot illustrates also an inertial zone's inclination of the kinetic energy spectrum in according with the Kolmogorov's law ($k^{-5/3}$) valid for 3D flows. The curve obtained with the Smagorinsky model posses a similar slap, showing the capacity of the 2D model to predict the energy distribution from the great to the minor scales presents in the flow.

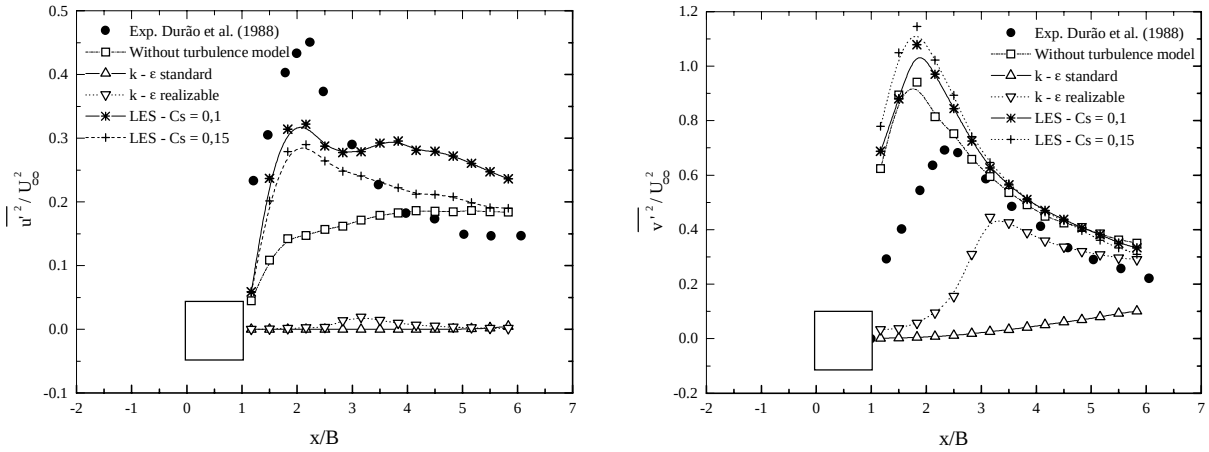

(a) Longitudinal velocity (b) Transversal velocity

Figure 3. Longitudinal and normal fluctuation velocity distribution on the centerline at $Re = 1.4 \times 10^4$.

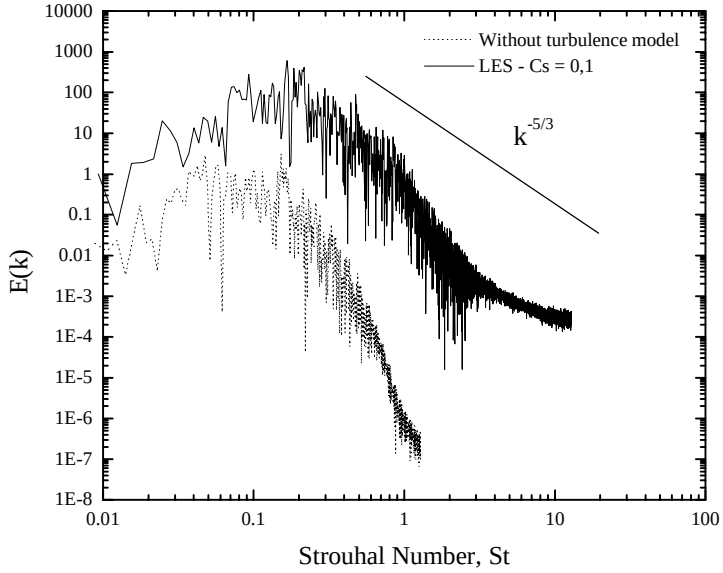

Figure 4. Energy spectrum obtained from the velocity signal acquired in the wake at $Re = 1.4 \times 10^4$.

4.2 Flow Regime at $Re = 2.2 \times 10^4$

This section presents the results obtained exclusively with Smagorinsky model for a Reynolds number equal to 2.2×10^4. The results with $Cs = 0{,}1$ were compared with another numerical and experimental ones.

Table 2 includes the computed values for the Strouhal number and mean drag coefficient. The simulation of Bouris & Bergeles (1999) is closer to the experimental value from Lyn *et al.* (1995) than the present work. However, in that work the grid size is more refined, with 300×350 resolution. In spite of this discrepancy, the other flow field variables were well predicted by the simulations of this work.

Tabela 2. Strouhal number of a square cylinder at $Re = 2.2 \times 10^4$.

Configuration		Strouhal	$\overline{Cd}$
Bouris & Bergeles (1999)	LES – $Cs = 0.1$	0.134	2.18
Present work	LES – $Cs = 0.1$	0.168	2.28
Lyn *et al.* (1995) – Experimental		0.135 – 0.139	2.05 – 2.23

Figure 5 shows the longitudinal velocity and the total kinetic energy distribution on the centerline only at downstream of the cylinder. For comparison effects other numerical results obtained with the LES methodology were inserted in this plot, as the tridimensional data of Murakami *et al.* (1992) and Breuer & Pourquie (1996).

It is interesting to observe that the results of present work in the Figure 5(a) are better than 3D LES calculations of Murakami *et al.* (1992), when compared with experimental data from Lin *et al.* (1995). In according with Bouris & Bergeles (1999) the 3D LES on its own does not guarantee good results. On the other hand, fine resolution in the two dimensional plane is still very important.

Figure 5(b) illustrates the total kinetic energy (periodic + turbulent) distribution on the centerline. Again, the present calculations show a closer agreement to the experimental measurements than the 3D calculation of Murakami *et al.* (1992). The results obtained with the *k*-ε model yielded a steady state solution for the flow field, as will be seen later by means of flow visualization results.

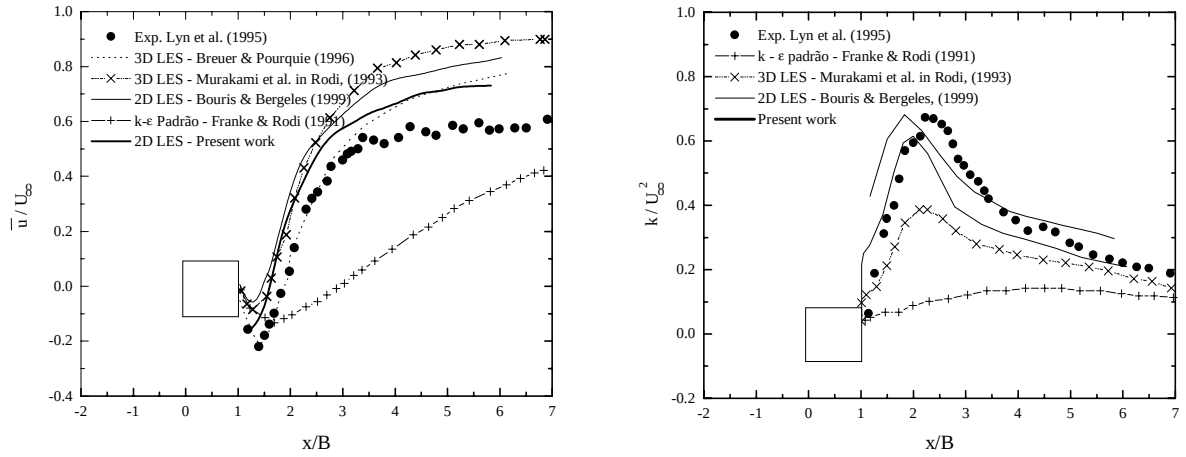

(a) Longitudinal velocity (b) Total kinetic energy

Figure 5. Longitudinal velocity and total kinetic energy distribution on the centerline at $Re = 2.2 \times 10^4$.

Figure 6 shows the energy spectrum obtained from the normal velocity fluctuation v' signal captured in the wake for the simulations with and without the Smagorinsky model. It is can be observed again that curve obtained with the Smagorinsky model concord very well with the inclination ($k^{-5/3}$) of the Kolmogorov's law.

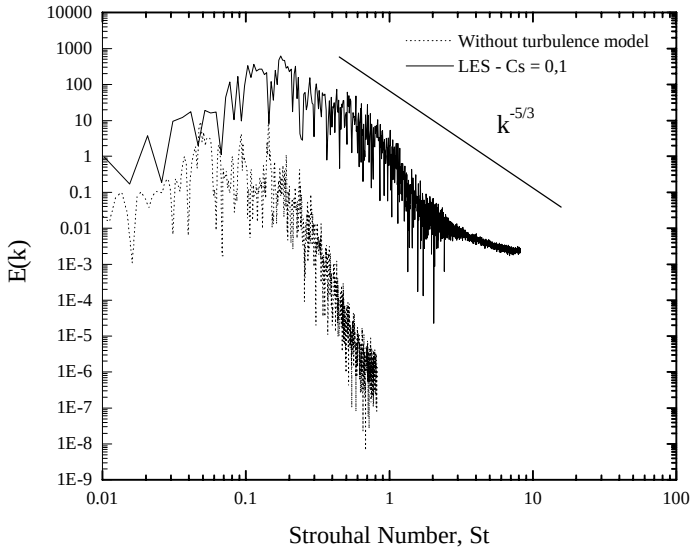

Figure 6. Energy spectrum obtained from the velocity signal acquired in the wake at $Re = 2.2 \times 10^4$.

4.3 Flowfield Visualization

The numerical visualization of the square cylinder's wake is showed, through the isovorticity plots, in the Figure 7 for a Reynolds equal to 1.4×10^4. As seen in the Figure 7(a) and 7(b), the LES computation presents a continuous vortex paring which are convected to downstream along the domain. It can also be observed a smaller formation region of the vortices behind the square cylinder with a pair of vortices shedding near of trailing corners, as indicated by the quantitative results shown in the Figure 2. The presence of the vortex pairing in the wake leads to frequent oscillations in the velocity signal having a strong influence in the determination of the fundamental vortex shedding, as noted in the quantitative results presented in the Table 1.

Figure 7(c) and 7(d) shows the numerical prediction obtained with *k*-ε models. As observed in the other numerical simulations – Franke & Rodi (1991) – the k-ε model used with wall functions fails to predict the cylinder's wake with no vortex shedding arising. In this work, the vortex shedding in the *k*-ε standard model begun at a dimensionless time of approximately equal to 500.

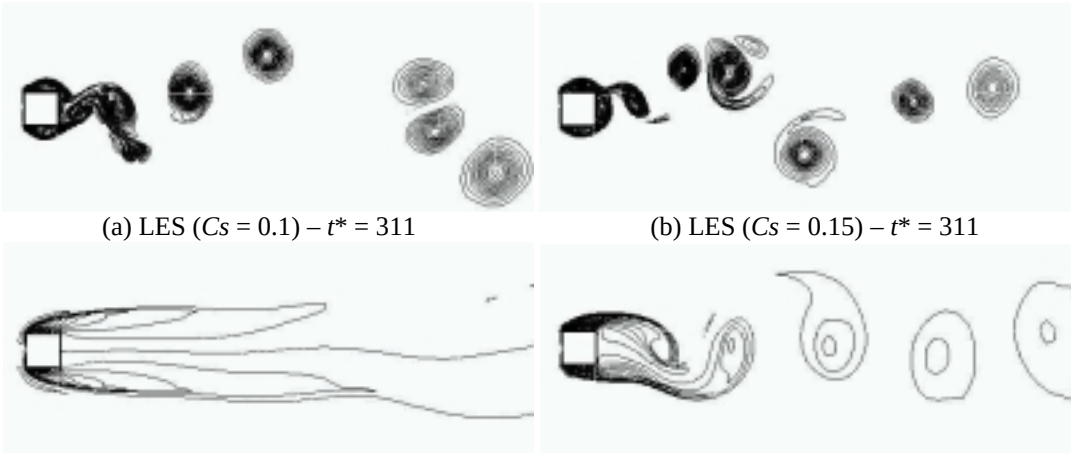

(a) LES (Cs = 0.1) – t^* = 311 (b) LES (Cs = 0.15) – t^* = 311

(c) *k*-ε standard – t^* = 311 (d) *k*-ε realizable – t^* = 311

Figure 7. The isovorticiy plots for the flowfield around a square cylinder with different turbulence models at $Re = 1.4\times10^4$.

The visualization of the wake for both *k*-ε models shows vortices regularly distributed along the von Kármán vortices street, as usually observed in the flow past around cylinders at low and moderate Reynolds number. In terms qualitative, the flow pattern obtained by LES simulations and *k*-ε models are quite different, although the quantitative results pointed to a better prediction of the flow field with the Smagorinsky LES model.

5. Concluding Remarks

This work presented the numerical bidimensional predictions of turbulent flow around a square cylinder at two relatively high Reynolds numbers. The calculations were carried out using Large Eddy Simulation (LES) methodology and classical modeling of turbulent flows via Reynolds average Navier-Stokes equations. In the LES case, the classical Smagorinsky model was employed setting the *ad-hoc* Smagorinsky constant for two different values. The k-ε simulations were accomplished with the standard and the realizable models.

Quantitative and qualitative results were used for testing the performance of the models. In general, both LES and classical simulations have provided a convenient global analysis of the flow field around the square cylinder. However, results from LES were able to reveal more sharp details on the flow motion and the periodic vortex shedding mechanism. On the other hand, the employ of LES methodology is much more exigent in terms of time processing and computational storage capability, in contrast with classical techniques using the k-ε models.

As a forecast, the notable advances in the computer's technology and numerical methods will quickly allow the use of Large Eddy Simulation methodology as an important tool to analysis of complex flows in severe turbulent regimes, replacing with advantages the classical modeling of the turbulence.

6. Acknowledgements

This study has been sponsored by FAPESP, under contract 97/12249-9 and 98/12990-3. The authors are also grateful to PROPP/UNESP and FUNDUNESP by the complementary financial support.

7. References

Durão, D. F. G., Heitor, M. V. & Pereira, J. C. F., 1988, Measurements of turbulent and periodic flows around a square cross-section cylinder, Experiments in Fluids, vol.6, pp.298-304.

Franke, R. & Rodi, W., 1991, Calculation of vortex shedding past a square cylinder with various turbulence models, in: Proc. 8th Symp. Turbulent Shear Flows, 9-11 September, Tech. Univ. Munich, Springer Berlin, pp.189-204.

Henkes, R. A. W. M., van der Flugt, F. F., Hoogendoorn, C. J., 1991, Natural Convection Flow in a Square Cavity Calculated with Low-Reynolds-Number Turbulence Models, Int. J. Heat Mass Transfer, 34:1543-1557.

Launder, B. E. & Spalding, D. B., 1974, The Numerical Computation of Turbulent Flows, Computer Methods in Applied Mechanics and Engineering, 3:269-289.

Lee, S., 1997, Unsteady aerodynamic force prediction on a square cylinder using k-ε turbulence models, Journal of Wind Engineering and Industrial Aerodynamics, vol.67/68, pp.79-90.

Leonard, B. P., 1979, A stable and accurate convective modelling procedure based on quadratic upstream interpolation, Comp. Meth. Appl. Mech. & Engng, pp.59-98.

Lyn, D. A., Einav, S., Rodi, W., Park, J. H., 1995, A laser-doppler velocimetry study of ensemble-averaged characteristics of the turbulent near wake of a square cylinder, Journal of Fluid Mechanics, vol.304, pp.285-319.

Murakami, S. & Iizuka, S., 1999, CFD analysis of turbulent flow past square cylinder using dynamic LES, Journal of Fluids and Structures, vol.13, pp.1097-1112.

Murakami, S., 1993, Comparison of various turbulence models applied to a bluff body, Journal of Wind Engineering and Industrial Aerodynamics, vol.46, pp.21-36.

Patankar, S. V. & Spalding, D. B., 1972, A calculation procedure for heat and mass transfer in three-dimensional parabolic flows, Journal of Heat and Mass Transfer, vol.15, pp.1787-1806.

Reynolds, W. C., 1987, Fundamentals of turbulence for turbulence modeling and simulation. Lecture Notes for Von Karman Institute Agard Report No. 755.

Rodi, W., 1993, On the simulation of turbulent flow past bluff bodies, Journal of Wind Engineering and Industrial Aerodynamics, vol.46/47, pp.3-19.

Sarkar, S., & Balakrishnan, L., 1990, Application of a Reynolds-Stress Turbulence Model to the Compressible Shear Layer, ICASE Report 90-18, NASA CR 182002.

Shih, T.H., Liou, W. W., Shabbir A., Zhu, J., 1995, A New k-e Eddy-Viscosity Model for High Reynolds Number Turbulent Flows - Model Development and Validation. Computers Fluids, 24(3):227-238.

Silveira-Neto, A., 1991, Simulation numérique des grandes echelles d'un ecoulement turbulent decollé en aval d'une marche, Tese de Doutorado – INPG – França.

Yu, D. & Kareem, A., 1997, Numerical simulation of flow around rectangular prism, Journal of Wind Engineering and Industrial Aerodynamics, vol.67/68, pp.195-208.